International Journal of Mass Spectrometry 311 (2012) 24–30

Contents lists available at SciVerse ScienceDirect

International Journal of Mass Spectrometry

journal homepage: www.elsevier.com/locate/ijms

Mass shift in the mass spectra of TOF-SIMS and the analysis of kinetic energies of the ions

Taisuke Nakanaga*, Hidekazu Nagai, Naoaki Saito, Yukio Fujiwara, Hidehiko Nonaka

National Institute of Advanced Industrial Science and Technology (AIST), Tsukuba Central 2, 1-1-1 Umezono, Tsukuba, Ibaraki 305-8568, Japan

ARTICLE INFO

Article history:
Received 23 May 2011
Received in revised form
25 November 2011
Accepted 25 November 2011
Available online 13 December 2011

Keywords:
CsI cluster ion
TOF-SIMS
Unimolecular dissociation reaction

ABSTRACT

The apparent mass shift of the CsI cluster ions $(CsI)_nCs^+$ and $(CsI)_nI^-$ observed in high resolution mass spectra by TOF-SIMS of CsI crystal has been investigated in terms of the kinetic energy of the ions. The sharp peak of CsI cluster ion showed apparent mass shifts, which cannot be corrected by usual method. The kinetic energy analysis has shown that the initial kinetic energy depends on the cluster size, and this is the reason for apparent mass shifts. The unimolecular dissociation of CsI cluster ion in field-free drift region that gives the broad peaks has been assigned by the analysis of the kinetic energies. The precursor ion $(CsI)_pCs^+$ or $(CsI)_pI^-$ emits one or two CsI units at a time and the branching ratio $R_p = k_{p\to p-2}/k_{p\to p-1}$ strongly depends on the cluster size. It becomes large when $p-2$ is the magic number (6, 9, 13) of the cluster ion, and small when $p = 7$. The result was compared with the DFT calculations.

1. Introduction

The use of cluster ion beams and static conditions is expected to lead the applications of the time-of-flight secondary ion mass spectrometry (TOF-SIMS) to the analyses of a variety of samples including functional polymers and biomaterials [1–4]. Since in TOF-SIMS the ion mass is indirectly determined by converting the measured traveling time of the ion, a calibration of the relationship between the measured time and the mass is essential. When an accuracy on the order of 10 ppm (parts per million) is required for the mass measurement, we need a standard sample which gives ions whose mass is the same order of the target ion and the chemical compositions can be determined easily. For this purpose organic molecules seem to be inadequate for the calibration in the high mass region because they tend to decompose to fragments, and it is hard to determine the chemical composition of these fragment ions when the mass is larger than 100 u/e. The inorganic compounds that consist of heavy atoms and no hydrogen atom seem to be suited for this purpose. We examined metal cluster complex and alkali halide cluster ions as the candidates for the standard sample, and found iridium cluster carbonyl complex $Ir_4(CO)_{12}$ can be used for the mass calibration in 1000–2000 u/e region [5].

It is well known that CsI gives large cluster ions [6,7], and there are many researches about the structure and reactions [8–14], and also there are studies about the mass calibration using CsI cluster ion [15,16]. In the case of the mass spectrum of CsI crystal measured by TOF-SIMS we observed the signals of CsI cluster ions in the wide mass range up to 10,000 u/e at every 260 u/e, however, almost all of them showed apparent mass shift and cannot be used as the mass standard [5]. The apparent peak shift seemed due to the effect of the reaction of the cluster ions. It seems useful to study the reactions of the CsI cluster ions in a apparatus of a high resolution TOF-SIMS for the search of other standard samples as a mass marker. The kinetic energy measurement gives useful information about the reactions. In the present work we measured the kinetic energy of the cluster ions by changing the post acceleration potential instead of controlling the reflector potential because the latter method gives critical effect on the performance of the high resolution TOF-SIMS. Present method does not give any critical effect on the high resolution TOF-SIMS except the relative intensity of the mass signal.

In this paper we measured the high resolution mass spectra of CsI crystal by TOF-SIMS. The effects of the reactions on the mass spectra have been analyzed considering the observed kinetic energies and the stabilities of the cluster ion calculated by the DFT method.

2. Experimental

A commercial optical crystal of CsI was used for the measurement. Using a TOF-SIMS system (TOF-SIMS 5 by Ion-TOF GmbH.), the mass spectra of the sample were measured by Toray Research Center as a commercial analysis service. The primary ion beam was reported to be Bi_3^{++} at 25 kV with a pulse width of 4.3 ns before bunching which yields high mass resolution of an order of ppm. Both positive and negative secondary ions were measured in the

* Corresponding author. Tel.: +81 29 861 2124; fax: +81 29 861 5301.
E-mail address: t.nakanaga@aist.go.jp (T. Nakanaga).

1387-3806/$ – see front matter © 2011 Elsevier B.V. All rights reserved.
doi:10.1016/j.ijms.2011.11.014

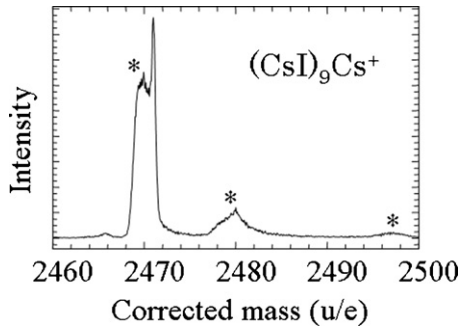

Fig. 1. A close-up of the mass spectrum of the CsI cluster ion around $M = 2470$. The sharp peak is assigned to the cluster ion $(CsI)_9Cs^+$. Three extra peaks indicated by * are assigned to the product ion of the unimolecular dissociations of the larger cluster ions.

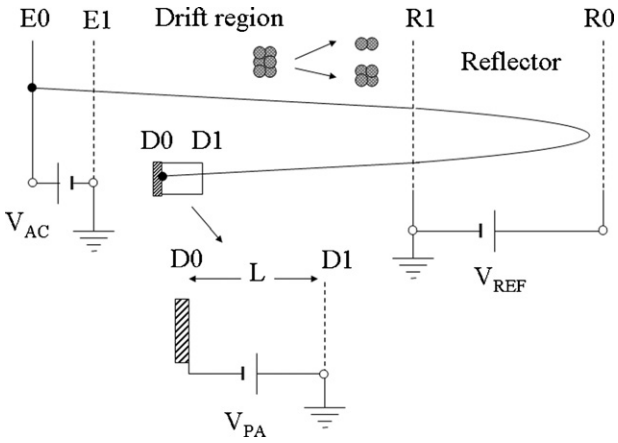

Fig. 2. Schematic diagram of the TOF-MS with a reflectron, and the origin of the broad peaks observed in the mass spectrum. $E_0, E_1, R_0, R_1, D_0, D_1$ are the electrodes. The product ions generated in the field-free drift region between E_1 and R_1 give the broad peaks.

mass range of 0–11,000 u/e. The acceleration voltage was 2 kV. Each spectrum was calibrated by means of extrapolation using the signals of Cs^+, $(CsI)_2Cs^+$, $(CsI)_4Cs^+$ for positive ion spectra and I^-, $(CsI)_2I^-$, $(CsI)_4I^-$ for negative ion spectra.

To achieve the high detection efficiency of the micro-channel-plate (MCP) detector, the TOF-SIMS system has post acceleration potential in front of the detector. Three values of the post acceleration potential, 2.5 kV, 5.0 kV and 10.0 kV, were used to determine the relative kinetic energies of the CsI cluster ions.

The stabilization energy and the structures of the most stable isomers of $(CsI)_nCs^+$ and $(CsI)_nI^-$ cluster ions were calculated using B3LYP method with LanL2DZ basis set (Gaussian 03 program [17]).

3. Results and discussion

3.1. TOF-SIMS spectra of CsI crystal

The broad overview of the TOF-SIMS positive ion spectrum of CsI was similar to that reported by Campana et al. [6]. The signals of $(CsI)_nCs^+$ cluster ion were observed up to 10,000 u/e. Since there is no isotope both for ^{133}Cs and ^{127}I, the mass spectrum is simple and signal peaks are observed at every 260 u/e. The famous magic numbers of $n = 9$, 13, 22 were clearly observed. The negative ion spectrum resembled to the positive ion spectrum. These features may suggest that CsI cluster ion can be used as a mass marker in the low resolution mass spectrometry. High resolution mass spectrum, however, showed that the spectrum is not so simple that CsI cluster ion cannot be used as a mass standard for the high resolution mass spectrometry [5].

Fig. 1 shows a close-up of the observed mass spectrum around 2480 u/e of a positive ion spectrum. A sharp peak is observed near the calculated mass of the cluster ion $(CsI)_9Cs^+$, and there are three extra broad peaks (indicated by * in Fig. 1) around the sharp peak. This kind of peaks is known to appear when the cluster ion dissociates in the free fright tube in the reflectron. A schematic diagram of the TOF-MS with a reflectron is shown in Fig. 2. Secondary ions are created at E_0 and accelerated in acceleration field between E_0 and E_1. They fly in field-free drift region between E_1 and R_1 and enter the reflector at R_1. They are reflected in the reflecting field, enter the field-free drift region at R_1 and finally reach to the detector. Let us consider unimolecular dissociation in the field-free drift region between E_1 and R_1, where the product ion is spontaneously generated from the precursor ion. Since the velocity of the product ion is almost the same as that of the precursor ion and constant in the field-free drift region, the flight time of the product ion does not depend on where the dissociation occurs between E_1 and R_1. The product ion has different stagnation time in the reflector from the precursor ion. These are the reason for the three extra peaks observed in Fig. 1. The extra peak becomes broad because the TOF-SIMS is optimized to achieve high mass resolution for the precursor ions and also there is a translational energy distribution of the product ion originated from the unimolecular dissociation.

These extra broad peaks cannot be used for the mass calibration. The disturbance of the broad peaks becomes serious as the cluster size n increases. Actually the sharp peak of $(CsI)_nCs^+$ with $n > 13$ was not recognized in the mass spectrum. This fact limits the available mass range of calibration with the sharp peaks of CsI cluster ion to less than 3000 u/e.

Apart from the disturbance by the broad peaks, the sharp peaks themselves also showed a problem that limited the usefulness of the CsI cluster ion as a standard sample. Fig. 3a shows the close-up of the sharp peaks of $(CsI)_nCs^+$ ($n = 0$–7). The vertical broken line shows the mass of the cluster ion calculated by the standard method in which the calibration was performed using the small ions observed in the low mass region. It is clear that there are apparent mass shifts in the peak positions. Fig. 3b summarizes the observed shift in the mass peaks for $n = 0$–9 of the positive ion. The error exceeds 50 ppm at 2000 u/e. We tried to fit the observed time

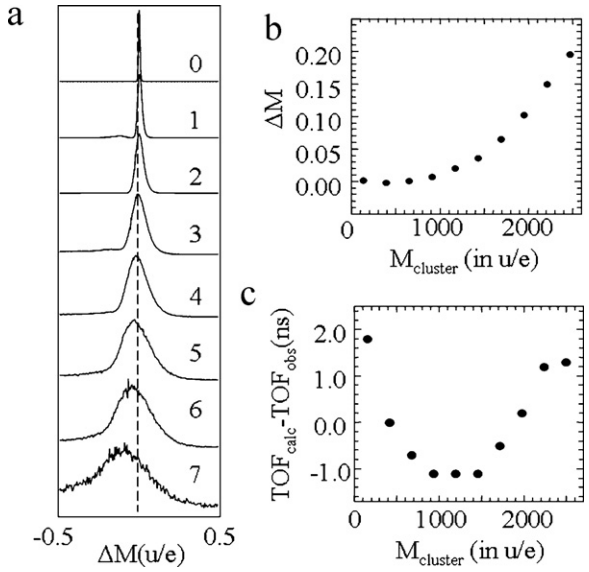

Fig. 3. The apparent mass shift of $(CsI)_nCs^+$ cluster ions observed in the mass spectrum of CsI crystal measured by TOF-SIMS. (a) Close-up mass spectra of the CsI clusters. (b) Deviations from the calculated values of the mass signals. (c) The residual error of the observed TOF to the standard equation $t - t_0 = k\sqrt{M}$.

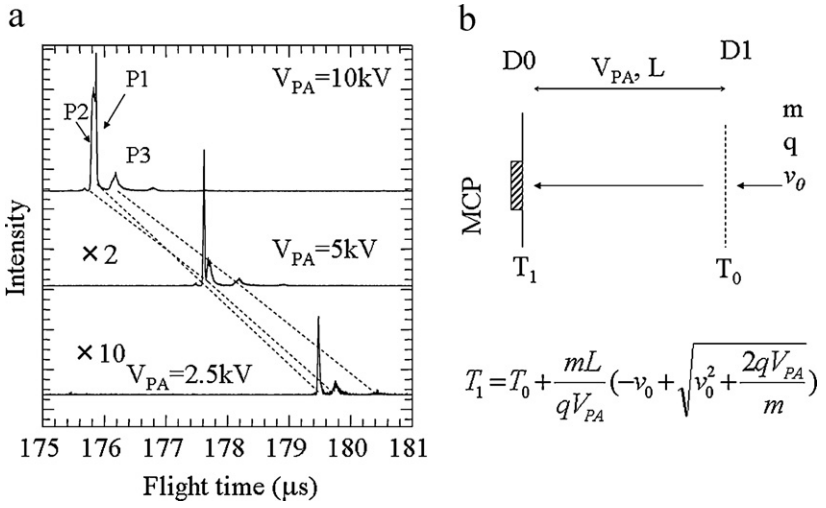

Fig. 4. (a) The effect of the post acceleration potential on the mass spectrum of CsI cluster ions measured by TOF-SIMS. Sharp peak (P1) is assigned to the $(CsI)_9Cs^+$ cluster ion. (b) A simple model of the post acceleration and flight time of the ion.

of flight (TOF) of the cluster ions $(CsI)_nCs^+$ (n = 0–9) to their mass (M) using the usual relation $t - t_0 = k\sqrt{M}$. Fig. 3c shows the residuals of the least square fit of the TOF to the equation. Apparently there is a systematic error which cannot be corrected by the standard method. This fact suggests that even the sharp peaks cannot be used for the mass calibration without making the origin of this shift clear. Similar apparent shifts of $(CsI)_nI^-$ were also observed in the negative ion spectrum.

3.2. The effect of the post acceleration potential in front of the detector and the kinetic energy of the ions

The post acceleration method is used to get high sensitivity of the MCP detector in the high mass region [18]. As shown in Fig. 2 the electrodes are set in front of the detector, and this electrodes can be used as a low resolution linear TOF or an energy analyzer of the ions. In the present work we estimated the kinetic energy of the cluster ions by changing the post acceleration potential instead of controlling the reflector potential because the latter method gives critical effect on the performance of the high resolution TOF-SIMS. Present method does not give any critical effect on the resolution of TOF-SIMS except the relative intensity of the mass signal is affected.

Fig. 4a shows the effect of the applied post acceleration potential in front of the detector on the mass spectrum of $(CsI)_9Cs^+$ region. The horizontal axis is TOF of the cluster ion in μs. In the figure, the series of peaks noted by P1 corresponds to the sharp peak observed near the mass position of $(CsI)_9Cs^+$. It is apparent that TOF became longer when lower PA voltage was applied, and also the change of TOF depends on the ion. To analyze the change of TOF, a simple model of the post acceleration was assumed as shown in Fig. 4b. TOF of a cluster ion whose mass is m and velocity at the entrance of the post acceleration electrode D_1 is v_0 is given by

$$T_1 - T_0 = \frac{mL_{PA}}{qV_{PA}}\left(-v_0 + \sqrt{v_0^2 + \frac{2qV_{PA}}{m}}\right), \quad (1)$$

where T_0 and T_1 is the time when the ion arrives at the entrance and MCP detector, respectively. L_{PA} is the distance between the entrance of the PA electrodes D_1 and the MCP detector and V_{PA} is the applied post acceleration voltage. L_{PA} was fixed to 117 mm taking the flight time of the small ions into account. The kinetic energy of small ions was calculated to be about 725 eV, which is considerably lower than the applied extraction potential of 2 kV. This inconsistency is due to the fact that the model used in the calculation was too simple. For example there may be a repulsive potential before the post acceleration electrodes to avoid the noise caused by the stray ions, which reduces the apparent kinetic energy. In the present work, we will use the simple model in Fig. 4b. The relative value of the kinetic energy seems to be still reliable even if we use this simple model.

In the analysis of the cluster ion, an appropriate value of n, the number of CsI molecules in the cluster, was assumed, and T_0 and v_0 were determined by least square fitting to the observed T_1 values. Then we adopted the cluster size n that gave the smallest residual of the least square fitting. Table 1 shows a part of the results of the analysis of the flight time of the cluster ions observed in Fig. 4a. The cluster size has been determined to be 9 for all three series P1–P3 observed in the TOF spectra in Fig. 4a. The kinetic energy of the ion that gives the sharp peak (P1) is determined to be 717 eV, which approximately agrees with that of the small ions in the low mass region (~725 eV). On the other hand the kinetic energies of the ions that give broad peaks are definitely smaller. This is explained by the unimolecular dissociation of the cluster ion in the field-free drift region.

When a cluster ion dissociates into two fragments, the product ion and neutral fragment, the kinetic energy of the product ion $KE_{product}$ is approximately proportional to the ratio of the mass of the product ion to its precursor ion,

$$KE_{product} \approx KE_{precursor}\left(\frac{M_{product}}{M_{precursor}}\right), \quad (2)$$

because the velocity of the product ion is almost the same as that of the precursor ion. As mentioned above the absolute value of the kinetic energy of the cluster ion determined by PA method is not necessary the same as the kinetic energy in the drift tube. For

Table 1
An example of the result of the least squares calculation of TOF of cluster cations.

Series	P1	P2	P3
T_0 (10 kV)/μs	175.8660	175.8218	176.1868
T_0 (5 kV)/μs	177.6212	177.7056	178.1916
T_0 (2.5 kV)/μs	179.4822	179.7640	180.4268
Res. (n = 9)	1.7	2.1	0.2
Res. (n = 8)	6.3	6.7	9.7
Res. (n = 10)	8.8	10.0	8.4
K.E./eV	717.5	579.8	475.6
$n_{precursor\ ion}$	9	10	11

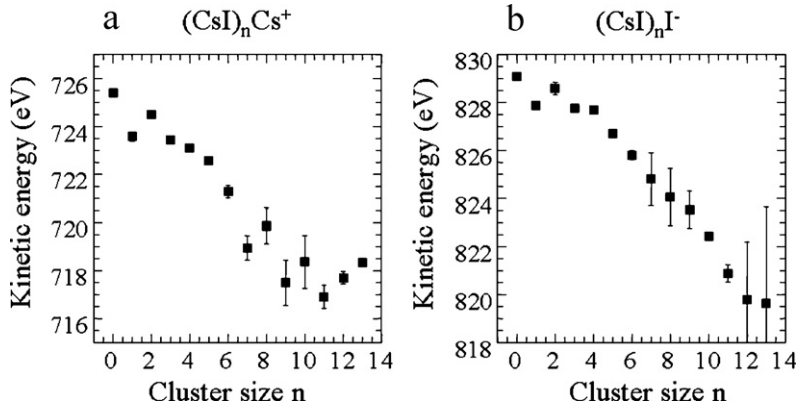

Fig. 5. The dependence of the kinetic energy of the $(CsI)_nCs^+$ and $(CsI)_nI^-$ cluster ions on the cluster size n. The absolute value is not important because it strongly depends on the settings of the apparatus.

example the barrier to eject the stray ions is neglected in the model calculation. If the K.E. in Table 1 is adjusted by the equation

$$KE_{product\,ion} = K.E. + 690 \quad (3)$$

the cluster sizes of the precursor ions are calculated to be integer values, 10 and 11, respectively for P2 and P3. Eq. (3) is also effective for all of the observed broad peaks of $(CsI)_nCs^+$ up to $n = 20$. This low kinetic energy actually seems due to the potential barrier to eject the stray ions in the apparatus. A similar analyses were also done for the negative ion clusters.

3.3. The apparent mass shift of the sharp peak of the cluster ion

As discussed in the previous chapter, the sharp peak of the cluster ion $(CsI)_nCs^+$ shows an apparent mass shift in TOF-SIMS (Fig. 3), and it cannot be corrected by the standard method. A similar shift was also observed in the negative ion spectrum. The magnitudes of the shifts were smaller than those observed in the positive ion spectra, but the apparent mass shifts also could not be corrected by the standard method.

In order to clarify the reason of the apparent mass shift, the kinetic energy of the cluster ion that gives the sharp peak in the mass spectrum has been estimated by the post acceleration method. Fig. 5a and b shows the results of the positive and negative ion clusters, respectively. The vertical bars show the standard deviation in the least squares calculations. The reliability of the data is actually limited by the line width of the mass signal. For the small clusters the accuracy is about 0.5 eV. It becomes worse with the increase of the cluster size to about 2 eV at $n \sim 9$. The reliability became worse in the larger clusters because the line becomes broad and overlapping by the broad peaks became serious. The absolute value of the kinetic energy depends on the settings of the apparatus as discussed in the early part of this paper, and not important for the present purpose.

It is interesting that the kinetic energy becomes lower with the increase of the cluster size. The kinetic energy of the small cluster ($n = 1$–3) is definitely higher than that of the larger clusters ($n = 9$–13) by about 8 eV. Comparison of the plots in Fig. 5 with the apparent mass shifts in Fig. 3b shows that there is a clear correlation between the kinetic energy and the cluster size. This is true also for the negative ion clusters. This fact strongly suggests that the origin of the apparent mass shift is the different kinetic energy of the cluster ions.

This kinetic energy dependence on the cluster size can be understood by the collision cascade model of the static SIMS [19]. Fig. 6 illustrates schematically the case of CsI. The temperature at the center of the primary ion bombardment rises much higher than that of the surrounding area where it is also elevated but rather moderate. To generate atomic ions or small cluster ions, high energy is required to break most of the bonds between the atoms. So these ions are expected to be generated at the high temperature region near the center of the ion bombardment. On the other hand larger cluster ions are generated at the peripheral region where the temperature is not high enough to break all the bonds. The kinetic energy of the secondary ion at the surface is one of the freedom of the translational energy, and it becomes high when the temperature of the surface is high.

3.4. Unimolecular dissociation of CsI cluster ion

Several authors studied the unimolecular dissociation reactions of $(CsI)_nCs^+$ cluster ions in various conditions and discussed the branching of the reactions[8–14]. Present results agreed with their results qualitatively, but PA method enables us to measure the unimolecular dissociation reactions of the cluster ions in the wide mass range under the same experimental conditions, and also it is easy to measure the reaction of the negative cluster ions. In this chapter, the branching ratio of the unimolecular dissociations of $(CsI)_nCs^+$ and $(CsI)_nI^-$ have been measured in the wide mass range under a similar experimental conditions, and the dependence of the ratios on the cluster size have been discussed.

As mentioned in the previous sections, we can determine the sizes of the precursor and the product ions of the unimolecular dissociations in the field-free drift region by measuring the kinetic

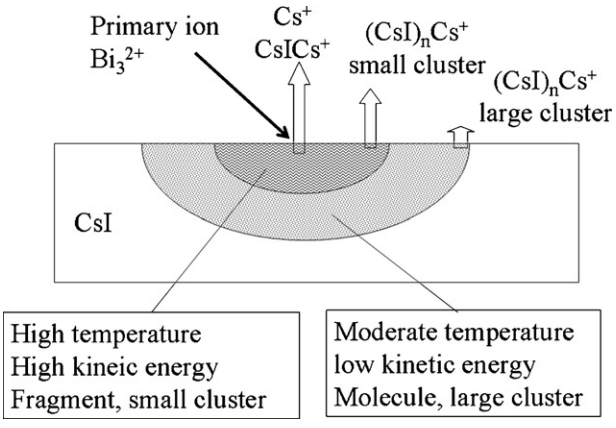

Fig. 6. A schematic explanation of the origin of the different kinetic energy observed for the CsI cluster ions. The temperature near the center of the bombardment becomes high, and small fragment ions are generated. In the surrounding area, the temperature moderately increase, and large cluster ions are generated.

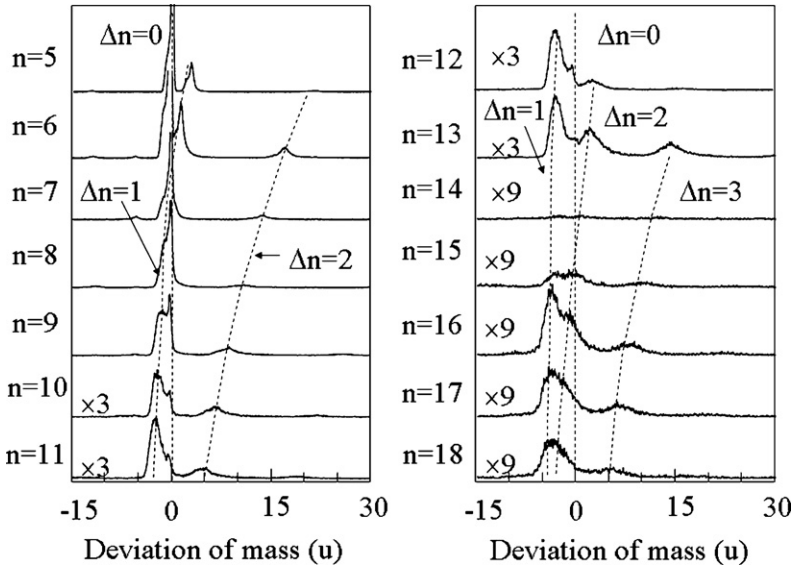

Fig. 7. The assignment of the broad peak to the unimolecular dissociation reactions of the cluster ions $(CsI)_pCs^+ \rightarrow (CsI)_nCs^+ + \Delta n CsI$ by the measurements of the kinetic energies of the corresponding ions. Note that the n represents the size of the product ion.

energies of the product ions. Fig. 7 summarizes the assignments of the fragment ions observed in the mass spectrum of the positive ion to the unimolecular dissociation reaction,

$$(CsI)_pCs^+ \rightarrow (CsI)_nCs^+ + \Delta n(CsI) \quad (4)$$

where p and n is the cluster size of the precursor and the product ion, respectively, and $\Delta n = p - n$ is the number of CsI units dissociated in the reaction. The assignments of p, n and Δn are made by the least square analysis similar to that shown in Table 1 for the cluster ions of $(CsI)_nCs^+$ for $n = 6$–16. It is interesting that the signals of the product ions appear near the calculated mass of the product ion. Since the velocity of the product ion should be significantly less than that of the secondary ion of the same mass which did not dissociate in the flight path, the flight time of the product ion could be much longer than that of the secondary ion. This is partly cancelled by the design of the reflector of the TOF-SIMS system in which the effect of the distribution of the kinetic energies of the secondary ions is minimized. Similar analyses were also made for the negative cluster ions $(CsI)_nI^-$, and the results were very similar to those of the positive cluster ions.

Present method enables us to determine the number of CsI molecules released from the precursor ion $(CsI)_pCs^+$ between the exit of the acceleration region (E_1 in Fig. 2, ≈2 μs after the primary ion bombardment) and the entrance of the reflector (R_1 in Fig. 2, ≈100 μs). In most cases, the number of CsI molecules released from the cluster ion is one or two. It is expected that $\Delta n = 2$ reaction is not the two-step reaction of $\Delta n = 1$ dissociation, because the $(CsI)_2$ dimer is stabilized by the dipole–dipole interaction and the two step reaction of $\Delta n = 1$ reaction needs large excess energy.

Fig. 8 shows the dependence of the branching ratio $I_{p\rightarrow p-2}/I_{p\rightarrow p-1}$, of the unimolecular dissociations on the cluster size of the precursor ion p

$$(CsI)_pCs^+ \rightarrow (CsI)_{p-1}Cs^+ + CsI \quad (5)$$

$$(CsI)_pCs^+ \rightarrow (CsI)_{p-2}Cs^+ + (CsI)_2 \quad (6)$$

for positive ion clusters, and

$$(CsI)_pI^- \rightarrow (CsI)_{p-1}I^- + CsI \quad (5')$$

$$(CsI)_pI^- \rightarrow (CsI)_{p-2}I^- + (CsI)_2 \quad (6')$$

for negative ion clusters. The relative intensity, $I_{p\rightarrow p-2}/I_{p\rightarrow p-1}$, was estimated from the signal intensity of the mass spectrum measured with the post acceleration potential $V_{PA} = 10$ kV. When the peaks overlapped with each other, the intensity was estimated from the mass spectra measured with $V_{PA} = 2.5$ kV and $V_{PA} = 5$ kV in which the corresponding peak was observed separately. The reliability of the branching ratio in Fig. 8 is limited by the sensitivity of the MCP detector, which depends on both the mass of the ions and the applied post acceleration potential [18]. In the present case the difference of the mass of the precursor and product ions is one or two CsI units, which is small compared with the total mass of the precursor ions. As long as the intensities measured with the same post acceleration potential were compared, the error originated from the sensitivity of MCP detector is expected to be less than a few ten percents.

It is interesting that both the positive and negative cluster ions show quantitatively same dependence of the branching ratio on the cluster size. This seems due to the fact that the ion radius of Cs^+ is not very different from that of I^- and the ionic interaction determine the structure and the nature of the CsI cluster ions.

In Fig. 8, the observed branching ratio $I_{p\rightarrow p-2}/I_{p\rightarrow p-1}$ takes maximum value at $p = 15$ and minimum value at $p = 7$. The large value at

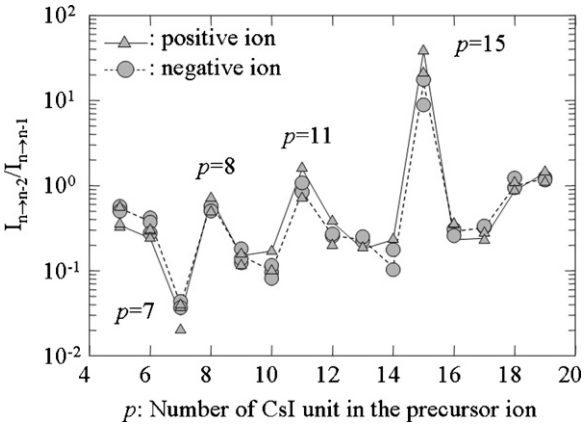

Fig. 8. The dependence of the branching ratio of the reactions of $(CsI)_pCs^+ \rightarrow (CsI)_{p-1}Cs^+ + CsI$ and $(CsI)_pCs^+ \rightarrow (CsI)_{p-2}Cs^+ + (CsI)_2$ on the cluster size of the precursor ion $(CsI)_pCs^+$.

$p = 15$ seems to be due to the stability of the cluster ion $(CsI)_{13}Cs^+$, the well-known magic number of the alkali halide clusters [6]. Similar peaks are also observed at $p = 8$ and $p = 11$, which also correspond to the magic number clusters of $(CsI)_6Cs^+$ and $(CsI)_9Cs^+$. From these facts the positive peak at p in the plot of the branching ratio suggest that $(CsI)_{p-2}Cs^+$ cluster is a stable cluster.

It is interesting that the branching ratio at $p = 14$ does not show large negative peak. Since $(CsI)_{13}Cs^+$ cluster is stable compared with other clusters, we could expect that the 14→13 reaction is much favored than 14→12 reaction, and that the branching ratio should have a minimum peak at $p = 14$. Actually this is not true, and perhaps the transition energy or other factors should be considered. A similar phenomenon is also found at $p = 10$. On the other hand the peak at $p = 8$ is somewhat different from the former two cases. There is a negative peak at $p = 7$. Considering the case of $p = 15$ and $p = 11$, the negative peak at $p = 7$ seems not due to the stability of $(CsI)_6Cs^+$ but due to the relative unstability of $(CsI)_5Cs^+$. In order to discuss the reaction more precisely, the stabilization energies of the clusters were calculated by DFT method.

3.5. DFT calculations of the CsI cluster ions

The structures and the energies of the most stable isomers of the cluster ions of $(CsI)_nCs^+$ and $(CsI)_nI^-$ up to $n = 17$ were calculated by using Gaussian 03 program [17]. The structures of the cluster ion whose cluster size n was less than 13 were optimized by the following way. Firstly some probable structures were assumed, and optimized them using HF method with CEP-4G basis set. Then the converged structures were again optimized using B3LYP method with LanL2DZ basis set. In the case of larger cluster ions ($n > 13$), the existence of the cubic unit $(CsI)_{13}Cs^+$ or $(CsI)_{13}I^-$ in the cluster was assumed in the first step, and optimization was performed in the same scheme as that used for the small cluster ions. As for the neutral clusters $(CsI)_n$ similar calculations were performed up to $n = 16$.

Aguado et al. reported the ab initio calculations of $(CsI)_nCs^+$ cluster ions ($n = 1$–14) [20] and recently Fernandez-Lima reported the DFT calculations of smaller cluster ions ($n = 1$–8) [21]. The calculations give the same structures for the most stable isomers of the positive ion cluster except for $(CsI)_5Cs^+$. The structure given by Aguado et al. slightly differed from the other two calculations. Since our calculation agreed with that given by Fernandez-Lima et al. the discrepancy seems due to the difference of the basis set or calculation method. Anyway the difference of the calculated energies of the two isomers is only 0.01 eV in our calculations, this difference will not affect the following discussions about the unimolecular dissociation reactions of the cluster ions.

The structures of the most stable isomers of the negative ion clusters $(CsI)_nI^-$ have been also calculated. The optimized structures are essentially the same as those of the positive ion clusters if the atoms Cs and I are replaced with each other. This seems due to the fact that the ion radius of Cs^+ is not very different from that of I^- and the ionic interaction determine the structure of the cluster ions. One exception is found at $n = 7$. Fig. 9a and b shows the most stable isomers of $(CsI)_7Cs^+$ and $(CsI)_7I^-$ cluster ions, respectively. The structure of $(CsI)_7Cs^+$ is slightly different from other clusters. It consists of two parts of cubic and hexagonal structures, and small change of ionic distance can make this structure unstable. The calculation shows, however, that the energy difference between the most and the second stable isomers is about 0.05 eV, which is much smaller than the difference of the stabilization energy (see Fig. 10).

The stabilization energy of the clusters were calculated as

$$E^+(n) = E((CsI)_nCs^+) - nE(CsI) - E(Cs^+) \quad (7)$$

$$E^-(n) = E((CsI)_nI^-) - nE(CsI) - E(I^-) \quad (8)$$

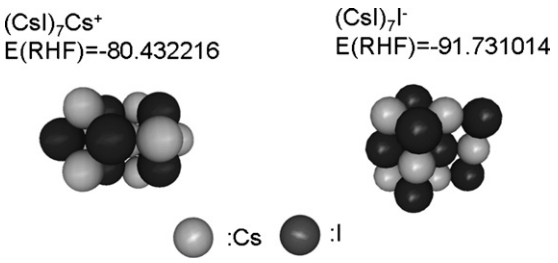

Fig. 9. The most stable isomers of cluster ions calculated by DFT method. (a) $(CsI)_7Cs^+$; (b) $(CsI)_nI^-$. The structure of the second stable isomer of positive ion resembles to that of the negative ion.

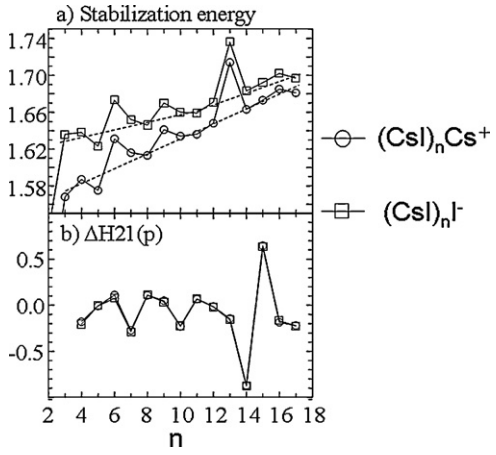

Fig. 10. (a) Calculated stabilization energy per CsI molecule of $(CsI)_nCs^+$ and $(CsI)_nI^-$. See text for the definitions. (b) The difference of the enthalpy change of the reactions of $\Delta n = 1$ and $\Delta n = 2$. There is no significant difference between the positive and negative cluster ions.

where $E((CsI)_nCs^+)$, $E((CsI)_nI^-)$, $E(CsI)$, $E(Cs^+)$, and $E(I^-)$ are the calculated energies of the cluster cation, cluster anion, CsI monomer, Cs^+ and I^-, respectively. Table 2 summarizes the calculated stabilization energy of $E(n)$ and also the stabilization energy per CsI unit, $EC(n)/n$ and $E(n)/n$. Fig. 10a shows the dependence of the stabilization energy of CsI cluster ions per CsI unit on the cluster size n. The feature of the magic numbers $n = 6, 9, 13$ is clearly observed in the plot. It is interesting that the stabilization energy of $(CsI)_5Cs^+$ is small compared with the neighboring clusters. These features coincide with the positive and the negative peaks in the branching

Table 2
Calculated stabilization energy and the enthalpy change (in eV).

n	$(CsI)_nCs^+$				$(CsI)_nI^-$			
	$\Delta E(n)$	$E(n)/n$	ΔE_1	ΔE_2	$\Delta E(n)$	$E(n)/n$	ΔE_1	ΔE_2
1	1.582	1.582			1.708	1.708		
2	2.886	1.443	1.304	1.247	3.064	1.532	1.356	1.425
3	4.703	1.568	1.817	1.482	4.907	1.636	1.843	1.560
4	6.349	1.587	1.646	1.824	6.551	1.638	1.644	1.848
5	7.876	1.575	1.527	1.534	8.114	1.623	1.563	1.569
6	9.785	1.631	1.909	1.797	10.038	1.673	1.924	1.848
7	11.314	1.616	1.529	1.799	11.565	1.652	1.527	1.812
8	12.903	1.613	1.589	1.479	13.167	1.646	1.602	1.490
9	14.771	1.641	1.867	1.817	15.028	1.670	1.861	1.824
10	16.342	1.634	1.571	1.800	16.596	1.660	1.568	1.790
11	17.994	1.636	1.652	1.584	18.253	1.659	1.656	1.585
12	19.777	1.648	1.784	1.796	20.050	1.671	1.797	1.814
13	22.287	1.714	2.510	2.654	22.564	1.736	2.514	2.672
14	23.278	1.663	0.991	1.862	23.569	1.683	1.005	1.880
15	25.100	1.673	1.822	1.174	25.375	1.692	1.806	1.172
16	26.958	1.685	1.859	2.041	27.237	1.702	1.862	2.029
17	28.570	1.681	1.612	1.831	28.854	1.697	1.618	1.840

ratio of the unimolecular dissociations of the cluster ions discussed in the previous section (Fig. 8).

To see the unimolecular reactions more precisely the difference of the enthalpy changes between two reactions $\Delta H_{21} = \Delta H_2 - \Delta H_1$, where ΔH_1 and ΔH_2 are the enthalpy changes of the $\Delta n = 1$ and $\Delta n = 2$ reactions, respectively, were calculated. Since the stabilization energy of the neutral dimer $(CsI)_2$ is 1.64 eV, which is about the same as that of CsI cluster ions, ΔH_{21} is small except the magic number cluster is concerned. Fig. 10b shows the dependence of ΔH_{21} on the cluster size. It is interesting that there is no significant difference between ΔH_{21} of the positive and negative ion clusters. This result agrees with the experimental result that there is no significant difference between the branching ratios of the positive and negative ion clusters (Fig. 8).

As expected from the stability of the magic number cluster $(CsI)_{13}Cs^+$, there is a large minimum at $n = 14$ and a large maximum at $n = 15$. If the unimolecular dissociation reactions are mainly controlled by the enthalpy difference, the plot should show the good correlation with that of the branching ratio. However as discussed earlier there is a maximum at $n = 15$ in the plot of the branching ratio, while the expected minimum at $n = 14$ is not clear. This fact suggests that the estimation of the entropy factor or investigation of more precise reaction mechanism is needed to understand the unimolecular dissociation reaction.

4. Conclusions

CsI cluster ion cannot be used as a mass marker for the high resolution mass spectrum measured by TOF-SIMS. In the high mass region (>3000 u/e), the original peak assignable to the secondary ion becomes very weak and overlapped by broad peaks due to the unimolecular dissociation of the cluster ions. Even in low mass region, it cannot be used as the mass marker because of the apparent mass shifts originated from the initial kinetic energy, or the conditions of the initial step of the generation of the secondary ion clusters.

The kinetic energy measurement by using post acceleration electrode has been probed to be a good tool for studying the reactions of the secondary ions including the unimolecular dissociation of the large cluster ions. The CsI cluster ion emits one or two CsI unit at a time, and the branching ratio shows the good correlation with the stability of the cluster ions.

Acknowledgement

This work has been supported by the Ministry of Economy, Trade and Industry.

References

[1] D. Briggs, D.M. Brewis, R.H. Dahm, I.W. Fletcher, Surf. Interface Anal. 35 (2003) 156–167.
[2] T. Kono, E. Iwase, Y. Kanamori, Appl. Surf. Sci. 255 (2008) 997–1000.
[3] H.F. Arlinghaus, Appl. Surf. Sci. 255 (2008) 1058–1063.
[4] J.-W. Park, H.-K. Shon, B.-C. Yoo, I.-H. Kim, D.-W. Moon, T.-G. Lee, Appl. Surf. Sci. 255 (2008) 1119–1122.
[5] H. Nonaka, T. Nakanaga, Y. Fujiwara, N. Saito, T. Fujimoto, Jpn. J. Appl. Phys. 49 (2010) 086601.
[6] J.E. Campana, T.M. Barlak, R.J. Colton, J.J. Decorpo, J.R. Wyatt, B.I. Dunlap, Phys. Rev. Lett. 47 (1981) 1046–1049.
[7] I. Katakuse, H. Nakabushi, T. IChihara, T. Sakurai, T. Matsuo, H. Matsuda, Int. J. Mass Spectrom. Ion Processes 57 (1984) 239–242.
[8] T.M. Barlak, J.R. Wyatt, R.J. Colton, J.J. Decorpo, J.E. Campana, J. Am. Chem. Soc. 104 (1982) 1212–1215.
[9] M.A. Baldwin, C.J. Proctor, 1-J. Amster, F.W. McLafferty, Int. J. Mass Spectrom. Ion Processes 54 (1983) 97–107.
[10] I.S. Katakuse, H. Nakabushi, T. IChihara, T. Sakurai, T. Matsuo, H. Matsuda, Int. J. Mass Spectrom. Ion Processes 62 (1984) 17–23.
[11] W. Ens, R. Beavis, K.G. Standing, Phys. Rev. Lett. 50 (1983) 27–30.
[12] J.E. Campana, B.N. Greed, J. Am. Chem. Soc. 106 (1984) 531–535.
[13] J.E. Campana, R.J. Colton, J.R. Wyatt, R.H. Bateman, B.N. Green, Appl. Spectrosc. 38 (1984) 430–432.
[14] R. Herzschuh, T. Drewello, Int. J. Mass Spectrom. 233 (2004) 355–359.
[15] E. Cornelis, C.A. Hop, J. Mass Spectrom. 31 (1996) 1314–1316.
[16] R. Hara, C. Sakabe, T. Ohwada, K. Yamaguchi, Bunseki Kagaku 53 (2004) 623–627.
[17] M.J. Frisch, G.W. Trucks, H.B. Schlegel, G.E. Scuseria, M.A. Robb, J.R. Cheeseman, J.A. Montgomery Jr., T. Vreven, K.N. Kudin, J.C. Burant, J.M. Millam, S.S. Iyengar, J. Tomasi, V. Barone, B. Mennucci, M. Cossi, G. Scalmani, N. Rega, G.A. Petersson, H. Nakatsuji, M. Hada, M. Ehara, K. Toyota, R. Fukuda, J. Hasegawa, M. Ishida, T. Nakajima, Y. Honda, O. Kitao, H. Nakai, M. Klene, X. Li, J.E. Knox, H.P. Hratchian, J.B. Cross, C. Adamo, J. Jaramillo, R. Gomperts, R.E. Stratmann, O. Yazyev, A.J. Austin, R. Cammi, C. Pomelli, J.W. Ochterski, P.Y. Ayala, K. Morokuma, G.A. Voth, P. Salvador, J.J. Dannenberg, V.G. Zakrzewski, S. Dapprich, A.D. Daniels, M.C. Strain, O. Farkas, D.K. Malick, A.D. Rabuck, K. Raghavachari, J.B. Foresman, J.V. Ortiz, Q. Cui, A.G. Baboul, S. Clifford, J. Cioslowski, B.B. Stefanov, G. Liu, A. Liashenko, P. Piskorz, I. Komaromi, R.L. Martin, D.J. Fox, T. Keith, M.A. Al-Laham, C.Y. Peng, A. Nanayakkara, M. Challacombe, P.M.W. Gill, B. Johnson, W. Chen, M.W. Wong, C. Gonzalez, J.A. Pople, Gaussian 03, Revision B.04, Gaussian, Inc., Pittsburgh, PA, 2003.
[18] I.S. Gilmore, M.P. Seah, Int. J. Mass Spectrom. 202 (2000) 217–229.
[19] P. Bertrand, L.T. Weng, Time-of-flight secondary ion mass spectrometry (ToF-SIMS), Mikrochim. Acta, Suppl. 13 (1996) 167–182.
[20] A. Aguado, A. Ayuela, J.M. Lopez, J.A. Alonso, Phys. Rev. B 58 (1998) 9972–9979.
[21] F.A. Fernandez-Lima, C. Becker, K. Gillig, W.K. Russell, M.A.C. Nascimento, D.H. Russell, J. Phys. Chem. A 112 (2008) 11061–11066.